Available online at www.sciencedirect.com
SCIENCE DIRECT®
Dyes and Pigments 57 (2002) 149–159
DYES and PIGMENTS
www.elsevier.com/locate/dyepig

# The crystalline-state photochromism, thermochromism and X-ray structural characterization of a new spiroxazine

Hee-Jung Suh[a], Woo-Taik Lim[b], Jian-Zhong Cui[a], Heung-Soo Lee[b], Ghyung-Hwa Kim[b], Nam-Ho Heo[c], Sung-Hoon Kim[a,*]

[a]*Department of Dyeing and Finishing, Kyungpook National University, Daegu 702-701, South Korea*
[b]*Pohang Accelerator Laboratory, Pohang University of Science and Technology, PO Box 125, Pohang 790-600, South Korea*
[c]*Department of Industrial Chemistry, Kyungpook National University, Daegu 702-701, South Korea*

Accepted 9 October 2002

**Abstract**

A new spiroxazine **4** was found to be photochromic and thermochromic both in solution and in the crystalline state. X-ray crystallography was used to determine that the molecules of the spiroxazine were arranged in a monoclinic (*C*2) crystallographic system. Intermolecular hydrogen bonds, together with interlayer, aromatic π–π stacking interactions, stabilize the molecular conformation and packing in the crystal structure.


*Keywords:* Spiroxazine; Crystalline-state photochromism; Thermochromism; X-ray crystallography; Monoclinic space group

## 1. Introduction

Photochromism has attracted much attention recently from the viewpoint of optical applications because of interest in refractive index or absorbance changes through optical excitation. The development of time-resolved or flash spectroscopy and, more recently, the use of laser photophysical analysis, has provided new ways of studying the excited states and transient species involved in the photoreactivity of photochromic molecules.

In recent years, photochromic and thermochromic spiropyrans and spiroxazines have received considerable attention due to their potentional application in many new technologies, such as data recording and storage, optical switching, displays and non-linear optics [1,2].

Although photochromic compounds have attracted significant attention because of their potential use as sunlight-activated, self-coloured glasses and optical memory media, they still await major commercial exploitation. One of the prime reasons for the lack of industrial applications for photochromic materials, particularly organic photochromic compounds, is their poor durability. Although the photochromism of spiropyran has been extensively studied [3,4], little research has been carried out on spiroxazine dyes. While these two classes of compounds are similar in many aspects, the replacement of the benzopyran ring by a naphthoxazine ring, which results in spironaphthoxazine, greatly improves resistance to

* Corresponding author. Tel.: +82-53-950-5641; fax : +82-53-950-6617.
*E-mail address:* shokim@knu.ac.kr (S.-H. Kim).

0143-7208/03/$ - see front matter © 2003 Published by Elsevier Science Ltd.
PII: S0143-7208(02)00124-9

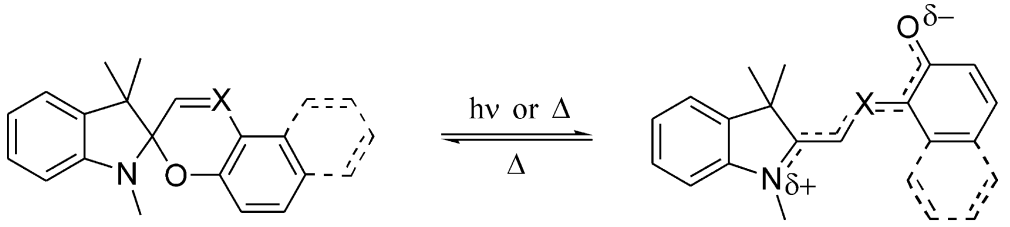


colorless form colored form

X = CH : spiropyran
X = N : spiroxazine

prolonged UV irradiation, which confers greater commercial importance [5].

We have preciously reported on the synthesis, photochromic properties and solvatochromic properties of spironaphthoxazines [6–8]. This paper concerns the synthesis, photochromism, thermochromism and crystal structure of a new spiroxazine which is substituted with a mesogenic group in the naphthalene ring.

## 2. Experimental

Melting points were determined using an Electrothermal IA 900 apparatus and were uncorrected. Elemental analyses were recorded on a Carlo Elba Model 1106 analyzer. Mass spectra were recorded on a Shimadzu QP-1000 spectrometer using an electron energy of 70 eV and the direct probe EI method. A multi-channel photodiode detector (MCPD, Otsuka Electronics) was used to obtain visible absorption spectra of spiroxazine in both the solution and crystalline states. $^1$H NMR spectra was recorded in $CDCl_3$ using a Varian Inova 400 MHz FT-NMR Spectrometer using TMS as internal standard.

### 2.1. Materials

1,3,3-Trimethyl-2-methylene-indoline (Fischer's base) and 2,7-dihydroxy-naphthalene were purchased from Fluka. 4-Butoxbenzoic acid, 1,3-dicyclohexyl-carbodiimide and 4-dimethylamino-

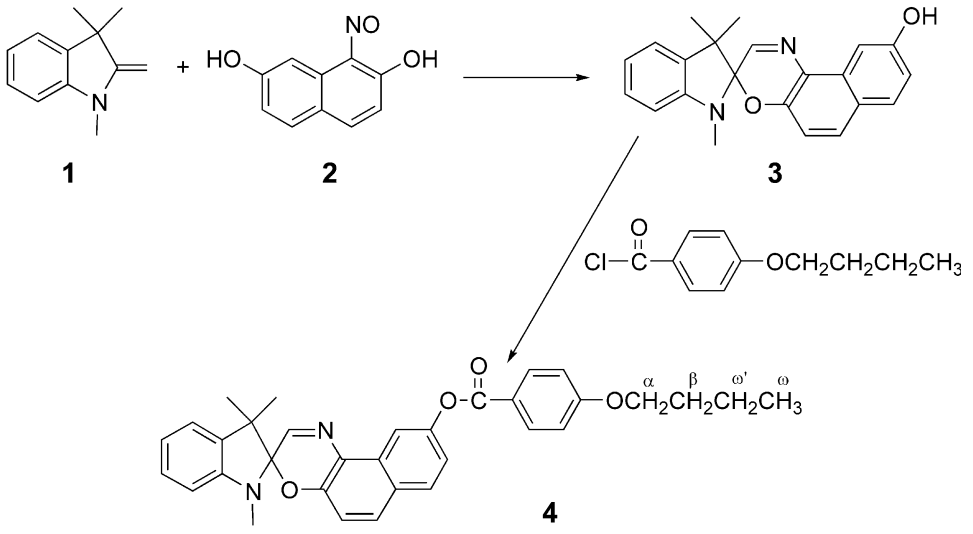

pyridine were purchased from Aldrich. All chemicals were of the highest grade available and were used without further purification.

### 2.2. Synthesis of 1,3,3-trimethyl-6′-hydroxyspiro-[2H]-indol-2,3′-[3H]-naphth[2,1-b][1,4] oxazine 3

1,3,3-Trimethyl-6′-hydroxyspiro[2H]-indol-2,3′-[3H]-naphth[2,1-b][1,4] oxazine **3** was prepared from 1,3,3-trimethyl-2-methylene-indoline **1** and 1-nitroso-2,7-dihydroxy-naphthalene **2** according to the method described in Refs. [9,10]. Yield 17.0 g (50%), mp. 211.5–214 °C. Elemental analysis: C; 76.89, H; 4.97, N; 8.59%. $C_{22}H_{20}N_2O_2$ requires: C; 76.72, H; 5.85, N; 8.13%.

Table 1
Crystal data and structure refinement

| | |
|---|---|
| Empirical formula | $C_{33}$ $H_{32}$ $N_2$ $O_4$ |
| Formula weight | 520.61 |
| Source | 6B, PAL (Pohang Accelerator Laboratory) |
| Temperature | 298(2) K |
| Wavelength | 1.0 Å |
| Crystal system, space group | Monoclinic, *C*2 |
| Unit cell dimensions | $a = 25.421(5)$ Å, $b = 8.298(2)$ Å, $c = 30.567(6)$ Å $\beta = 111.51(3)^\circ$ |
| Volume | 5999(2) Å$^3$ |
| *Z* | 8 |
| Calculated density | 1.153 Mg/m$^3$ |
| Absorption coefficient | 0.076 mm$^{-1}$ |
| F(000) | 2208 |
| Crystal size | 0.07×0.01×0.08 mm$^3$ |
| Resolution range (Å) | 20∼0.98 |
| $\theta$ range for data collection | 1.4–30.2° |
| Completeness ($>1\sigma$) (%) | 95.2 (83.7) |
| $R_{sym}$ (%) | 2.3 (8.1)[a] |
| $1/\sigma(I)$ | 60.6 (16.9) |
| Refinement method | Full-matrix least-squares on $F^2$ |
| Data/restraints/parameters | 2200/1/705 |
| Final *R* indices [$I > 2\sigma(I)$] | $R_1 = 0.1043$[b], $wR_2 = 0.2785$[c] |
| *R* indices (all data) | $R_1 = 0.1059$[b], $wR_2 = 0.2817$[c] |
| Goodness-of-fit on $F^2$ | 1.582[d] |

[a] $R_{sym} = \sum |I_{obs} - I_{avg}|/I_{obs}$, where $I_{obs}$ is the observed intensity of an indiuvidual reflection and $I_{avg}$ is the average over symmetry equivalents.

[b] $R_1 = \sum ||F_o| - |F_c|| / \sum |F_o|$

[c] $wR_2 = \left(\sum w|F_o - F_c|\right)^2 / \sum wF_o^2)^{1/2}$

[d] Goodness-of-fit $= \left\{\sum \left[w\left(F_o^2 - F_c^2\right)^2\right]/(n-p)\right\}^{1/2}$, where $n$ = number of reflections and $p$ = total number of parameters refined.

### 2.3. Synthesis of spiroxazine 4

4-Butoxybenzoic acid (1.0 g, 5 mmol) and thionyl chloride (1.2 g, 10 mmol) were refluxed for 3 h; excess thionyl chloride was then removed by distillation under reduced pressure. The 4-butoxybenzylcarbonyl chloride obtained was dissolved in 30 ml tetrahydrofuran and dropped into a stirred solution of compound **3** (1.7 g, 5 mmol) in 30 ml tetrahydrofuran containing 0.50 g (5 mmol) triethylamine, with the temperature mainitained below 0 °C with an ice bath. The ensuing solution was continuously stirred for 2 h at 0 °C and then several hours at a room temperature, before being filtered to remove the solid triethylamine hydrochloride salt. The remaining filtrate was evaporated under reduced pressure.

The product obtained was washed with ethanol several times and recrystallized from acetone and ethanol. Yield 2.4 g (93%), mp. 156–159 °C. Elemental analysis: found C; 75.70, H; 6. 56, N; 5.14. $C_{33}H_{32}N_2O_4$ requires: C; 76.13, H; 6.20, N; 5.38%. $M^+$ 520. $^1$H NMR ($CDCl_3$): 1.01 (3H, t, H(ω)), 1.348 (3H, s), 1.352 (3H, s), 1.54 (2H, m, H(ω′)), 1.83 (2H, m, H(β)), 2.77 (3H, s), 4.07 (2H, t, J = 6.5 Hz, H(α)), 6.58 (1H, d, $J = 7.8$ Hz), 6.90 (1H, t), 6.99 (3H), 7.09 (1H, d, $J = 7.1$ Hz), 7.22 (1H, m), 7.26 (1H, m), 7.62 (1H, d, $J = 8.8$ Hz), 7.71 (1H, s), 7.79 (1H, d, $J = 8.8$ Hz), 8.19 (2H, d, $J = 8.8$ Hz), 8.35 (1H, d, $J = 2.2$ Hz).

### 2.4. X-ray crystallographic analysis

Preliminary experiments and data collection for X-ray crystal structure determination were performed using synchrotron radiation produced from Beamline 6B at Pohang Accelerator Laboratory (PAL), Pohang, Korea. A small single crystal (0.07×0.01×0.08 mm$^3$) was glued to a glass fiber using epoxy resin. Analysis programs DENZO and SCALE-PACK were used for data reduction and scaling.

Unit cell parameters and systematic absences indicated a monoclinic space group *C*2 (No. 5)

with unit cell dimensions $a = 25.421(5)$ Å, $b = 8.298(2)$ Å, $c = 30.567(6)$ Å, $\beta = 111.51(3)^\circ$ and $Z = 8$. Data collection was carried out on a MacScience DIP2030b imaging plate, two-dimensional area detector using Si(111)-monochromated radition. $2\theta_{max} = 60.4^\circ$. Crystal structure was resolved and refined using a full-matrix, least-square procedure (SHELXL97) which resulted in final $R_1$ and $wR_2$ indices of 0.1043 and 0.2785, respectively [11]. All non-hydrogen atoms were refined anisotropically; hydrogen atoms were included in idealized positions with isotropic thermal parameters riding on those of the parent carbon atoms.

The crystallographic data are summarized in Table 1 and the final structural parameters are presented in Table 2; the selected bond distances

Table 2
Atomic coordinates ($\times 10^4$) and equivalent isotropic displacement parameters ($A^2 \times 10^3$)

| Atom | $x$ | $y$ | $z$ | $U$(eq) |
|---|---|---|---|---|
| O(1) | 3449(4) | 4546(13) | −1029(4) | 84(3) |
| O(2) | 3987(4) | 3452(14) | 1438(4) | 78(3) |
| O(3) | 3427(5) | 1538(17) | 1482(4) | 114(4) |
| O(4) | 5322(4) | 723(12) | 3485(4) | 82(3) |
| N(1) | 4198(6) | 4350(2) | −1298(6) | 111(5) |
| N(2) | 4153(6) | 3390(17) | −150(4) | 94(4) |
| C(1) | 3878(6) | 3850(3) | −1770(6) | 104(8) |
| C(2) | 3875(8) | 4550(2) | −2164(7) | 91(5) |
| C(3) | 3583(7) | 3910(3) | −2592(7) | 91(5) |
| C(4) | 3253(8) | 2630(3) | −2628(7) | 102(6) |
| C(5) | 3267(5) | 1844(19) | −2203(7) | 81(5) |
| C(6) | 3586(6) | 2422(15) | −1775(6) | 66(5) |
| C(7) | 3679(5) | 2008(18) | −1295(5) | 68(4) |
| C(8) | 3897(5) | 3470(2) | −1009(4) | 63(4) |
| C(9) | 4522(14) | 5500(7) | −1138(8) | 350(4) |
| C(10) | 3188(6) | 1150(2) | −1195(7) | 123(7) |
| C(11) | 4152(7) | 640(2) | −1118(6) | 116(6) |
| C(12) | 4293(6) | 3050(3) | −508(6) | 110(7) |
| C(13) | 3611(5) | 4026(19) | −210(6) | 79(5) |
| C(14) | 3280(5) | 4604(18) | −665(5) | 62(4) |
| C(15) | 2777(6) | 5350(2) | −706(6) | 88(5) |
| C(16) | 2621(5) | 5570(2) | −330(8) | 80(5) |
| C(17) | 2936(5) | 4984(18) | 109(6) | 64(4) |
| C(18) | 3443(7) | 4263(17) | 195(6) | 75(5) |
| C(19) | 3802(6) | 3570(19) | 647(7) | 64(4) |
| C(20) | 3626(6) | 3940(2) | 1012(7) | 79(5) |
| C(21) | 3120(7) | 4620(2) | 926(5) | 72(4) |
| C(22) | 2775(5) | 5170(2) | 487(7) | 95(6) |
| C(23) | 3864(6) | 2220(2) | 1676(6) | 84(5) |
| C(24) | 4251(6) | 1905(15) | 2132(5) | 57(4) |
| C(25) | 4766(6) | 2630(19) | 2328(5) | 71(4) |
| C(26) | 5114(5) | 2379(17) | 2767(6) | 70(4) |
| C(27) | 4992(6) | 1223(17) | 3039(6) | 83(5) |
| C(28) | 4495(6) | 385(18) | 2856(5) | 81(4) |
| C(29) | 4125(6) | 720(2) | 2419(7) | 88(5) |
| C(30) | 5821(7) | 1520(3) | 3741(6) | 107(6) |
| C(31) | 6086(6) | 960(2) | 4208(7) | 84(5) |
| C(32) | 5790(8) | 1340(3) | 4492(6) | 118(7) |
| C(33) | 6071(9) | 890(3) | 4987(7) | 165(10) |

$U$(eq) is defined as one third of the trace of the orthogonalized $U_{ij}$ tensor.

Table 3
Selected bond lengths (Å)

| | | | |
|---|---|---|---|
| O(1)–C(14) | 1.331(14) | C(8)–C(12) | 1.533(18) |
| O(1)–C(8) | 1.432(15) | C(13)–C(14) | 1.419(19) |
| O(2)–C(23) | 1.35(2) | C(13)–C(18) | 1.463(18) |
| O(2)–C(20) | 1.352(16) | C(14)–C(15) | 1.38(2) |
| O(3)–C(23) | 1.192(16) | C(15)–C(16) | 1.360(19) |
| O(4)–C(27) | 1.376(16) | C(16)–C(17) | 1.375(17) |
| O(4)–C(30) | 1.389(17) | C(17)–C(18) | 1.358(17) |
| N(1)–C(9) | 1.24(4) | C(17)–C(22) | 1.369(18) |
| N(1)–C(1) | 1.43(2) | C(18)–C(19) | 1.47(2) |
| N(1)–C(8) | 1.55(2) | C(19)–C(20) | 1.380(19) |
| N(2)–C(12) | 1.300(19) | C(20)–C(21) | 1.340(19) |
| N(2)–C(13) | 1.423(18) | C(21)–C(22) | 1.384(19) |
| C(1)–C(6) | 1.40(3) | C(23)–C(24) | 1.41(2) |
| C(1)–C(2) | 1.33(2) | C(24)–C(25) | 1.362(17) |
| C(2)–C(3) | 1.35(2) | C(24)–C(29) | 1.43(2) |
| C(3)–C(4) | 1.33(3) | C(25)–C(26) | 1.323(19) |
| C(4)–C(5) | 1.45(2) | C(26)–C(27) | 1.38(2) |
| C(5)–C(6) | 1.35(2) | C(27)–C(28) | 1.370(17) |
| C(6)–C(7) | 1.438(18) | C(28)–C(29) | 1.352(18) |
| C(7)–C(8) | 1.48(2) | C(30)–C(31) | 1.41(2) |
| C(7)–C(10) | 1.56(2) | C(31)–C(32) | 1.38(2) |
| C(7)–C(11) | 1.60(2) | C(32)–C(33) | 1.46(2) |

and bond angles are tabulated in Table 3 and 4, respectively. The structure model was drawn using an ORTEP(III) plotting program and is shown in Fig. 8.

## 3. Results and discussion

### 3.1. Photochromism

The photochromic reaction in question is caused by the reversible heterolytic cleavage of the C(spiro)–O bond under UV irradiation, yielding the coloured form that can return to the colourless form by ring closure under visible light irradiation or in the dark. Electronic absorption spectral changes of spiroxazine **4** upon UV irradiation in toluene are depicted in Fig. 1. The original spectral pattern was reversibly recovered within 7 s. The new band is ascribable to the generation of the open merocyanine form from the closed spiro form. Spectra measured after UV irradiation are proportional to each other in the visible region, indicating that only one species was formed. This allowed the absorption to be monitored at $\lambda_{max}$ (595 nm) as a function of time to obtain the thermal colour fading rate ($k$) of the transformation from the open merocyanine form to closed sipro form via a first-order reaction [Eq. (1)]:

$$A_t - A_\infty = A_i \bullet \exp(-kt) \quad (1)$$

where $A_i$ is the absorbance at 595 nm, $A_t$ the absorbance at 595 nm at time $t$ after UV irradiation. $A_\infty$ and $k$ refer to the absorbance at 595 nm after 1 h and first-order colour changing rate constant, respectively. In this thermal colour change process, the kinetic analysis predicts the logarithm of the difference between $A_\infty$ and $A_t$ at time $t$ to be linear with time, the slope giving the decolouration rate constant, $k$. First-order plots according to Eq. (1) for the spiroxazine dye **4** are shown in Fig. 2. The colour change rate constant $k = 36.3 \times 10^{-2}$ s$^{-1}$ was obtained from the slope.

Irradiation of a crystalline spiroxazine **4** was carried out using an ultra-thin pressed pellet. The UV–vis absorption spectra after different irradiation times are shown in Fig. 3. Upon UV irradiation, a broad absorption band appeared at around 610 nm which increased with increasing irradiation time. When the sample was left in the dark at

Table 4
Selected bond angles (°)

| | | | |
|---|---|---|---|
| C(14)–O(1)–C(8) | 118.9(10) | O(1)–C(14)–C(15) | 120.8(13) |
| C(23)–O(2)–C(20) | 122.3(12) | O(1)–C(14)–C(13) | 123.2(12) |
| C(27)–O(4)–C(30) | 120.9(12) | C(15)–C(14)–C(13) | 115.8(15) |
| C(9)–N(1)–C(1) | 131.8(18) | C(16)–C(15)–C(14) | 122.0(13) |
| C(9)–N(1)–C(8) | 122.3(19) | C(15)–C(16)–C(17) | 122.2(14) |
| C(1)–N(1)–C(8) | 102.9(15) | C(18)–C(17)–C(22) | 116.4(15) |
| C(12)–N(2)–C(13) | 121.6(12) | C(18)–C(17)–C(16) | 121.0(15) |
| C(6)–C(1)–C(2) | 122.2(14) | C(22)–C(17)–C(16) | 122.6(14) |
| C(6)–C(1)–N(1) | 110.8(19) | C(17)–C(18)–C(13) | 116.6(16) |
| C(2)–C(1)–N(1) | 127(2) | C(17)–C(18)–C(19) | 125.0(15) |
| C(3)–C(2)–C(1) | 121.4(19) | C(13)–C(18)–C(19) | 118.1(15) |
| C(4)–C(3)–C(2) | 120.0(17) | C(20)–C(19)–C(18) | 113.6(15) |
| C(3)–C(4)–C(5) | 118.6(18) | C(21)–C(20)–O(2) | 125.2(17) |
| C(6)–C(5)–C(4) | 121.3(16) | C(21)–C(20)–C(19) | 120.6(13) |
| C(5)–C(6)–C(1) | 116.1(15) | O(2)–C(20)–C(19) | 114.1(15) |
| C(5)–C(6)–C(7) | 136.0(14) | C(20)–C(21)–C(22) | 123.4(13) |
| C(1)–C(6)–C(7) | 107.7(14) | C(21)–C(22)–C(17) | 120.1(14) |
| C(6)–C(7)–C(8) | 107.0(13) | O(3)–C(23)–O(2) | 116.6(15) |
| C(6)–C(7)–C(10) | 117.6(13) | O(3)–C(23)–C(24) | 126.2(16) |
| C(8)–C(7)–C(10) | 114.3(13) | O(2)–C(23)–C(24) | 117.2(13) |
| C(6)–C(7)–C(11) | 109.7(10) | C(23)–C(24)–C(25) | 124.3(13) |
| C(8)–C(7)–C(11) | 108.1(10) | C(23)–C(24)–C(29) | 120.2(13) |
| C(10)–C(7)–C(11) | 99.4(12) | C(25)–C(24)–C(29) | 115.4(12) |
| O(1)–C(8)–C(7) | 111.6(10) | C(26)–C(25)–C(24) | 123.6(13) |
| O(1)–C(8)–N(1) | 103.5(12) | C(25)–C(26)–C(27) | 120.4(12) |
| C(7)–C(8)–N(1) | 101.8(11) | O(4)–C(27)–C(28) | 112.8(14) |
| O(1)–C(8)–C(12) | 113.9(12) | O(4)–C(27)–C(26) | 128.2(13) |
| C(7)–C(8)–C(12) | 111.8(14) | C(28)–C(27)–C(26) | 119.0(13) |
| N(1)–C(8)–C(12) | 113.3(12) | C(27)–C(28)–C(29) | 120.1(13) |
| N(2)–C(12)–C(8) | 120.5(12) | C(24)–C(29)–C(28) | 121.1(12) |
| C(14)–C(13)–N(2) | 116.7(15) | O(4)–C(30)–C(31) | 114.3(16) |
| C(14)–C(13)–C(18) | 122.1(14) | C(32)–C(31)–C(30) | 113.3(16) |
| N(2)–C(13)–C(18) | 120.6(13) | C(31)–C(32)–C(33) | 115(2) |

room temperature after irradiation, the absorbance at 610 nm decreased slowly. The first-order decolouration rate constant ($k = 1.44 \times 10^{-2}$ s$^{-1}$) in the crystalline state was smaller than that of in solution, which indicates that open-to-close occurs more readily in solution than in the crystalline state (Fig. 4).

### 3.2. Thermochromism

The nature of the colored form of spiropyrans and spiroxazines in solution has been discussed widely. The thermochromic mechanism which operates in these classes of dye has been assumed to involve a thermally sensitive equilibrium between the colourless spiro form and the open merocyanine structure obtained after the scission of the C–O bond.

The absorption intensity increased with increasing temperature, showing that the spiroxazine **4** exhibited thermochromic behaviour in both the solution and crystalline states (Figs. 5 and 6).

As the temperature increased, the colourless crystal turned blue due to the formation of merocyanine.

The enthalpy of reaction was determined by measuring the absorbance of the open form at several temperatures, according to the van't Hoff equation, Eq. (2):

$$\mathrm{d}\ln K/\mathrm{d}(1/T) = \mathrm{d}\ln A/\mathrm{d}(1/T) = -\Delta H/R \qquad (2)$$

Plots of ln $A$ *vs* $1/T$ are shown in Fig. 7.

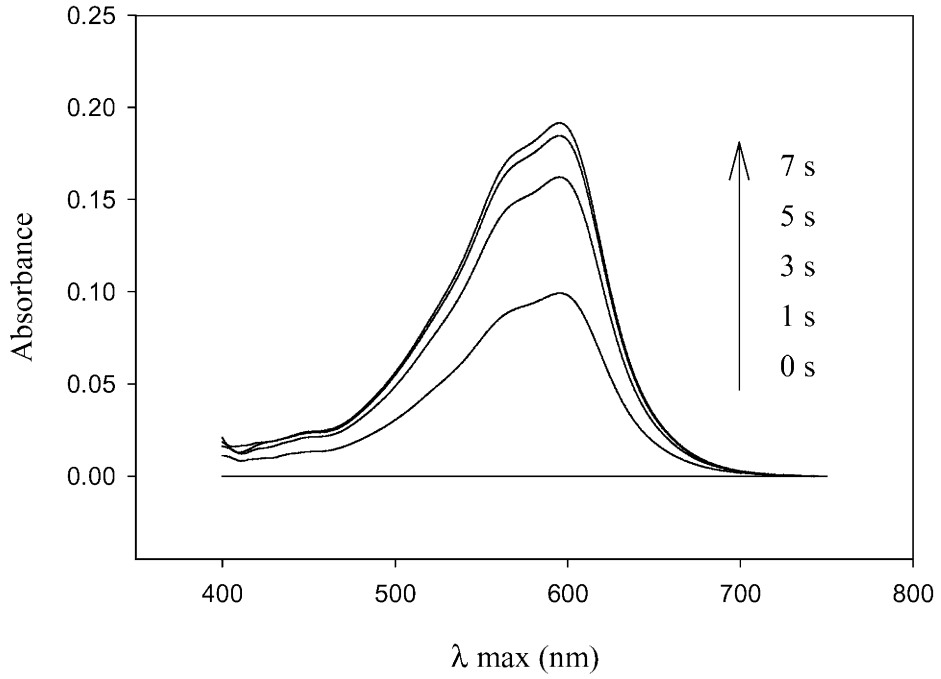


Fig. 1. Visible spectral changes of spiroxazine **4** in toluene solution ($8.2\times10^{-3}$ M, room temperature) upon UV irradiation.

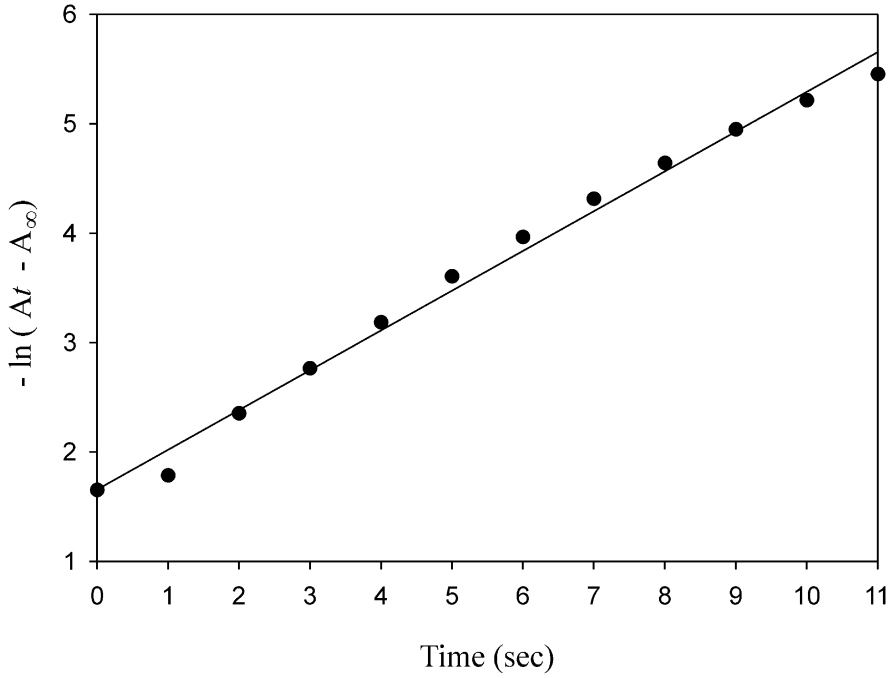


Fig. 2. Plot of $-\ln(A_t - A_\infty)$ as a function of time according to Eq. (1) for the decolouration of spiroxazine **4**.

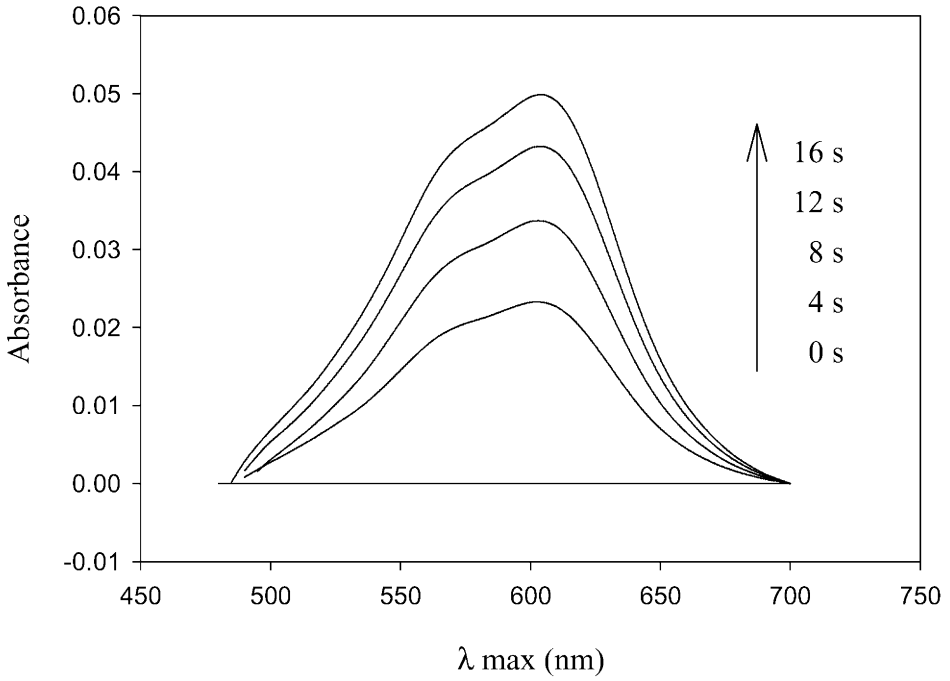


Fig. 3. Visible spectral changes of spiroxazine **4** in crystalline state.

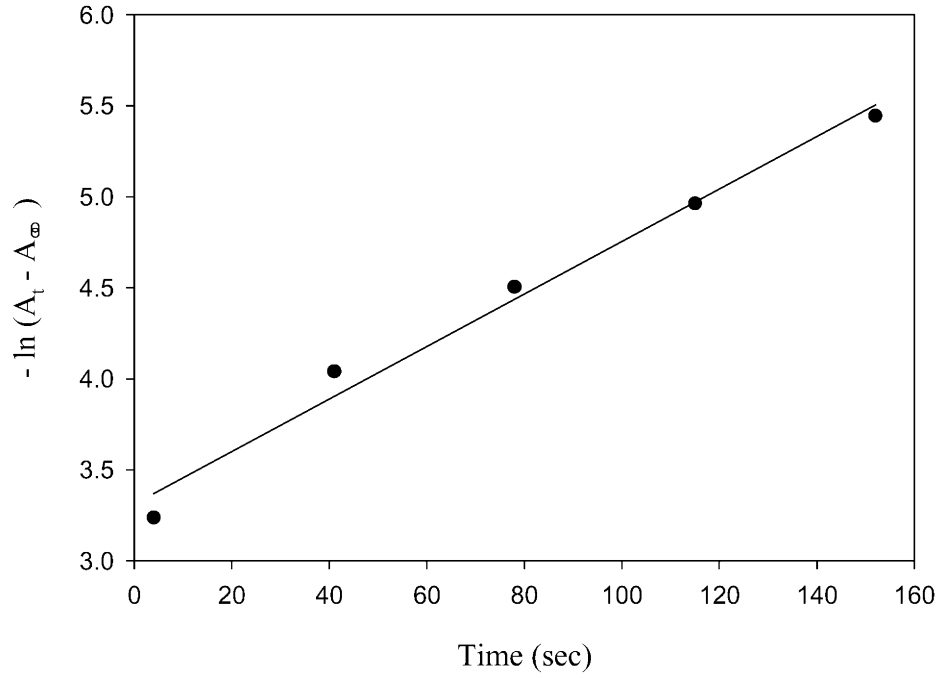


Fig. 4. Plot of $-\ln(A_t - A_\infty)$ as a function of time according to Eq. (1) for the decolouration of crystalline-state spiroxazine **4**.

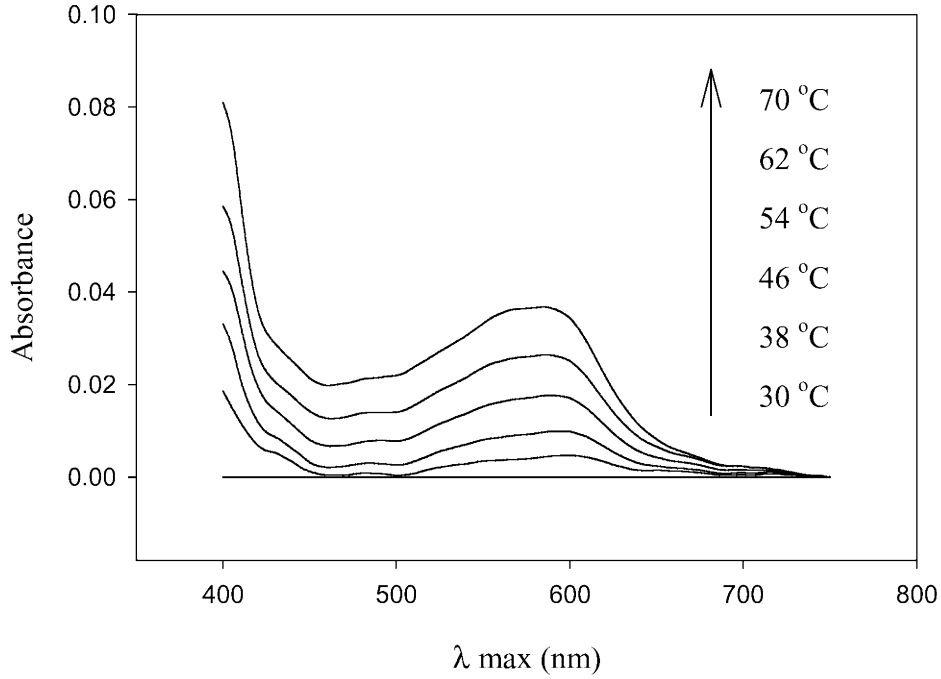


Fig. 5. Optical absorbance of spiroxazine **4** at various temperature in the region of the thermochromic band in toluene ($8.2\times10^{-3}$ M).

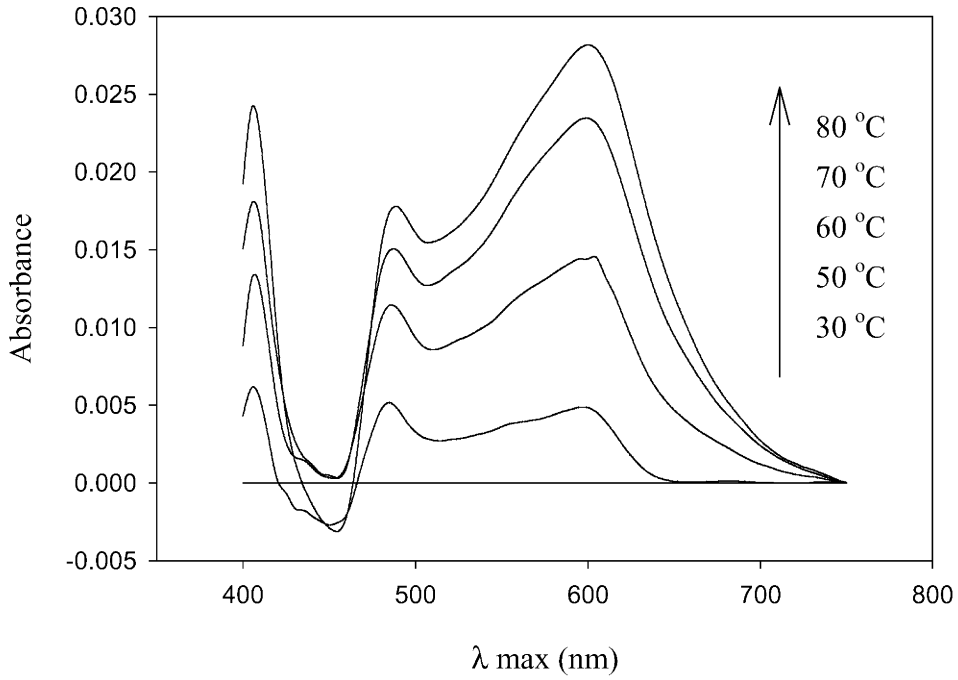


Fig. 6. Optical absorbance of crystalline-state spiroxazine **4** at various temperatures in the region of the thermochromic band.

In the above equation, the slope of the straight line of ln $A$ versus $1/T$ equals $-\Delta H/R$. The observation that a smaller $\Delta H$ value (52.27 kJ/mol) was obtained in toluene than in DMF (54.88 kJ/mol) is attributable to stabilization of the open merocyanine form in the nonpolar toluene. The finding that $\Delta H$ (132 kJ/mol) for the crystalline state thermochromism was higher than that for solution indicates that the energy difference between the spiro form and the open merocyanine form in the solid state thermochromism is larger than that of solution state thermochromism.

### 3.3. X-ray structural characterization

As it is fairly difficult to determine, experimentally, the structure of the open form, the X-ray structure of the closed form of spiroxazine **4** was determined, the final $R$ factors being $R_1 = 0.1043$ and $wR_2 = 0.2785$. It is evident that the molecules

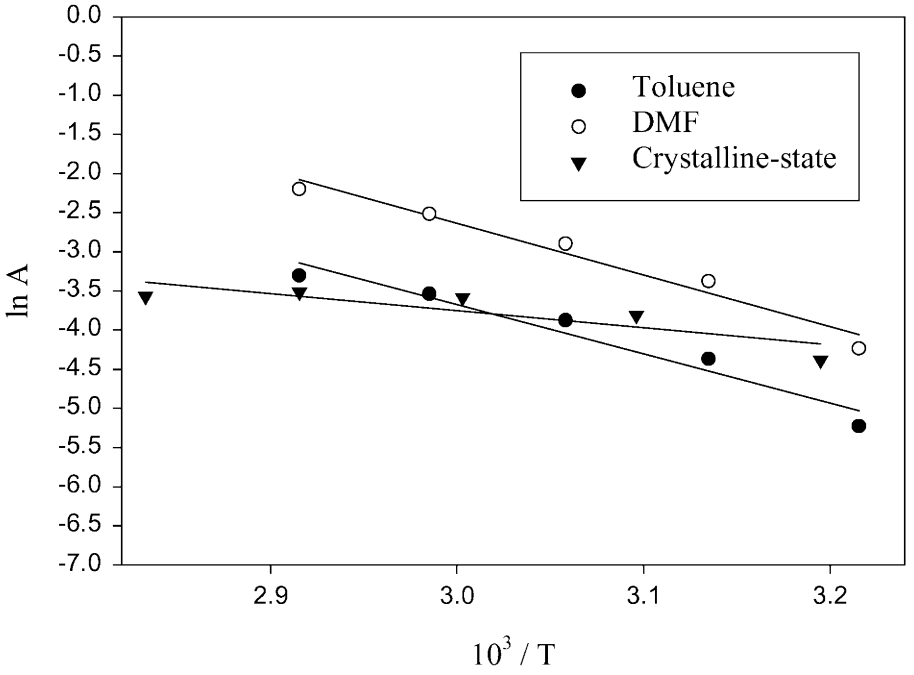


Fig. 7. Data for the thermal equilibrium treated according to the van't Hoff equation.

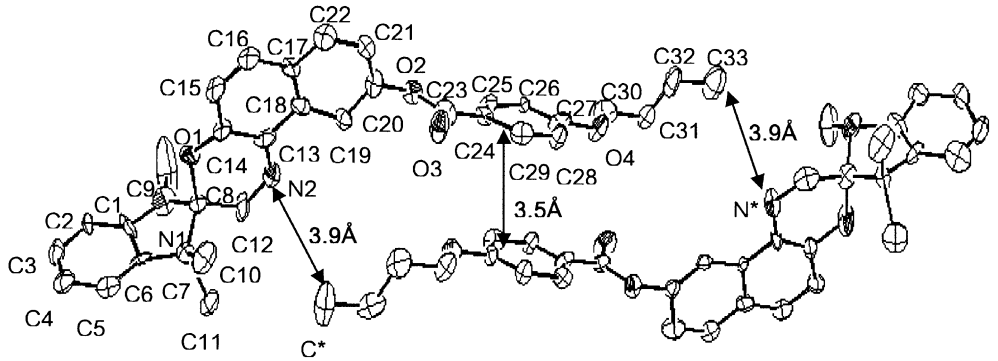


Fig. 8. ORTEP view of molecular structure of spiroxazine **4**.

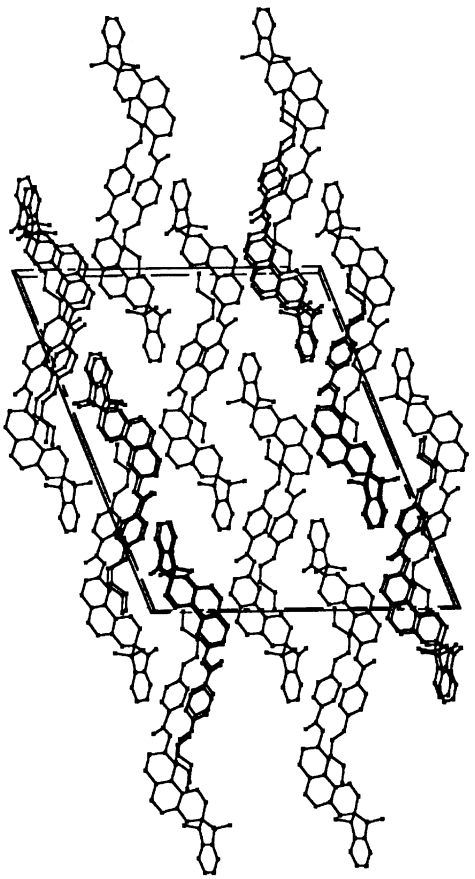

Fig. 9. Crystal packing structure in unit cell.

of the spiroxazine arrange themselves in a monoclinic crystallographic system ($C2$), unit cell of dimensions: $a = 25.421$, $b = 8.298$, $c = 30.567$ Å with $\beta = 111.51(3)^\circ$.

This closed form transforms to the coloured open form upon UV irradiation. From the ORTEP diagram, it was concluded that the spiro centre was tetrahedral (Fig. 8). The crystal packing scheme is shown in Fig. 9. Only the phenyl groups overlapped with face-to-face geometry, with an interplanar separation of 3.5 Å, the molecules being held together by π–π stacking interaction. The general hydrogen bond is constituted with a donor X-H and an acceptor A, in the form X-H—A. The bond may be described in terms of $d$, the distance between H—A, and $D$, the distance between X—A. The weak C-H—O hydrogen bonds have $d$ and $D$ separations of around 2.0–3.0 Å and 3.0–4.0 Å, respectively [12]. From the results of the intermolecular distance N2–C33 = 3.9 Å, the molecules are also held together through weak intermolecular hydrogen bonding.

## Acknowledgements

This research was supported by Kyungpook National University Research Fund, 2002 and was supported by the grant Post-Doctoral Program, Kyungpook National University (2001). Experiments at PLS were supported in part by MOST and POSCO.

## References

[1] Brown GH. Photochromism. New York: Wiley; 1971.
[2] Aramaki S, Atkinson GH. Journal of the American Chemical Society 1992;114:438.
[3] Kawauchi S, Yoshida H, Yamashita N, Ohira M, Saeda S, Werie MI. Bulletin of Chemical Society of Japan 1990; 63:267.
[4] Reeves DA, Wilkinson F. Journal of Chemical Society, Faraday Transition 1973;69:1341.
[5] Okudahira T. Seni Kakkaishi Japan 1992;48:253.
[6] Kim SH, Lee SN. Chemistry Express 1992;7:849.
[7] Kim SH, Park LS, Kim DJ, Kil KJ, Jung SC. Chemistry Express 1993;7:713.
[8] Kim SH, Park SJ, Song KH. Chemistry Express 1993; 8:741.
[9] Kakishita T, Matsumoto K, Kiyotsukuri T, Matsumura K, Hosoda M. Journal of Heterocyclic Chemistry 1992; 29:1709.
[10] Dürr H, Ma Y, Corterllaro G. Synthesis 1995:294.
[11] Sheldrick GM. SHELXL 97, program for the refinement of crystal structures. Germany: University of Gottingen; 1997.
[12] Desiraju G R, Steiner T. The weak hydrogen bond. Oxford University Press; 1999.